AD_____

Award Number: DAMD17-03-1-0657

TITLE: Multiple Aperture Radiation Therapy (MART) for Breast Cancer

PRINCIPAL INVESTIGATOR: Zhenyu Shou, Ph.D.

CONTRACTING ORGANIZATION: Leland Stanford Junior University
Stanford, CA 94305-4125

REPORT DATE: November 2004

TYPE OF REPORT: Annual Summary

PREPARED FOR: U.S. Army Medical Research and Materiel Command
Fort Detrick, Maryland 21702-5012

REPORT DOCUMENTATION PAGE

Form Approved
OMB No. 074-0188

1. AGENCY USE ONLY (Leave blank)	2. REPORT DATE	3. REPORT TYPE AND DATES COVERED
	November 2004	Annual Summary (1 Nov 2003 - 31 Oct 2004)

4. TITLE AND SUBTITLE
Multiple Aperture Radiation Therapy (MART) for Breast Cancer

5. FUNDING NUMBERS
DAMD17-03-1-0657

6. AUTHOR(S)

Zhenyu Shou, Ph.D.

7. PERFORMING ORGANIZATION NAME(S) AND ADDRESS(ES)

Leland Stanford Junior University
Stanford, CA 94305-4125

E-Mail: zhenyu@reyes.stanford.edu

8. PERFORMING ORGANIZATION REPORT NUMBER

9. SPONSORING / MONITORING AGENCY NAME(S) AND ADDRESS(ES)

U.S. Army Medical Research and Materiel Command
Fort Detrick, Maryland 21702-5012

10. SPONSORING / MONITORING AGENCY REPORT NUMBER

11. SUPPLEMENTARY NOTES

12a. DISTRIBUTION / AVAILABILITY STATEMENT
Approved for Public Release; Distribution Unlimited

12b. DISTRIBUTION CODE

13. ABSTRACT (Maximum 200 Words)

Not Provided

14. SUBJECT TERMS
Breast Cancer

15. NUMBER OF PAGES
38

16. PRICE CODE

17. SECURITY CLASSIFICATION OF REPORT	18. SECURITY CLASSIFICATION OF THIS PAGE	19. SECURITY CLASSIFICATION OF ABSTRACT	20. LIMITATION OF ABSTRACT
Unclassified	Unclassified	Unclassified	Unlimited

Table of Contents

I. INTRODUCTION

This postdoctoral fellowship grant (DAMD17-03-1-0657, entitled "Multiple Aperture Radiation Therapy for Breast Cancer") was awarded to the principal investigator (PI) for the period of Nov. 1, 2003—Oct. 31, 2005. This is the annual report for the first funding period (Nov. 1, 2003 –Oct. 31, 2004). The goal of this project is to develop a novel technique, Multiple Aperture Radiation Therapy (MART), as a candidate modality for treating breast cancer. The specific aims of this work are: (a) To demonstrate that MART can lead to substantially improved dose distribution over the conventional method, without increasing the complexity of the radiation treatment; (b) To show that the superior dose distributions of MART can be realized efficiently and accurately. Under the generous support from the U.S. Army Medical Research and Materiel Command (AMRMC), the PI has gained a tremendous amount of knowledge on breast cancer and breast cancer management over the last year. The support has also made it possible for the PI to contribute significantly to breast cancer research. A number of conference abstracts and a refereed paper has been resulted from the support. In this report, the past year's research activities of the PI are summarized.

II. RESEARCH AND ACCOMPLISHMENTS

II.1 Background

Radiation therapy is accepted as an effective treatment modality in the management of both invasive and non-invasive breast cancer[1-4]. Conventional breast radiotherapy utilizes two opposed tangential photon beams with either uniform or wedged shaped fluence profiles. A certain volume of the ipsilateral lung and, in the case of the left breast, a small volume of the heart is inevitably included in the tangential field, resulting in high radiation dose to this part of the lung and heart. For large sized breast, the technique is frequently incapable of producing homogeneous dose distribution in the target volume. Consequently, breast irradiation has been associated with a number of potential complications associated[5-8], including radiation induced pneumonitis, cardiac toxicity, rib fracture, arm edema, severe breast or chest wall fibrosis, and soft tissue or bone necrosis, and radiation induced secondary cancer. Adjuvant treatment with chemotherapy may further aggravate these effects.

Many approaches have been proposed to improve the current tangential-field treatment aiming at achieving more homogeneous dose distributions in the breast target volume and limiting radiation dose to normal structures to reduce cardiac and pulmonary toxicity. This includes the use of matched electron and photon beams to reduce dose to the underlying structures[9], the combination of conventional electron field and intensity-modulated photon beams[10], the irradiation using fan-beam and cone-beam intensity-modulated radiation therapy (IMRT) fields[11-14]. Each of these methods has pros and cons. The challenge is how to enhance the dose conformality without increasing the complexity of the treatment planning and delivery procedures. We have used a commercial inverse planning system (Corvus, North American Scientific, Cranberry Township, PA) to plan a number of breast treatments. While the advantage of IMRT with opposed tangential fields (OTF) for breast cancer is clear, the clinical implementation of the technique in a busy clinical environment is problematic. Indeed, the current IMRT planning and treatment process deviates significantly from the conventional approach and requires additional steps in planning and quality assurance (QA). For instance, in current system requires for a physician to segment explicitly the target volume, which wastes the physician's time (our estimate is ~20 minutes per patient) and increases the cost of health care. The inverse planning algorithm is not specially designed for breast planning and may not be the most efficient optimization scheme. In addition, the procedure of dosimetric verification of an arbitrarily shaped intensity-modulated beam is also not well established and the effort and quality of QA are also of great concern. In short, an effective method to plan and deliver IMRT breast treatment is highly desired in order for tens of thousands of breast cancer patients to benefit from the state-of-the-art technology.

The problems mentioned above can be solved naturally by MART approach. Generally speaking, there are two aspects in conformal radiation treatment planning: conformance of a certain dose to the target

volume and the dose uniformity inside the target. For simple beam configurations (eg., OTF, AP/PA), the dose conformation to the target volume is usually realized through beam shaping based on the initial MLC segments. In this case, MART technique obtained by adding a few segments to the original incident beams is often a viable choice to improve the target dose uniformity. The dose conformance here is realized by the proper choice of the initial tangential fields. The main purpose of introducing additional segments is to improve the dose homogeneity inside the target volume and/or to spare the sensitive structure(s) located along the path of the beams. Toward the general goal of establishing MART for breast cancer irradiation, we have (i) developed a manual MART planning procedure and assessed the dosimetric improvement resulted from MART; (ii) evaluated the number of segment dependence of the MART plans; (iii) developed a software tool that concatenates multiple segments for step-and-shoot delivery; (iv) constructed a dosimetric phantom that is capable of simulating the patient's breathing motion; (v) improved current inverse planning framework by introducing a voxel dependent penalty scheme and demonstrated its superiority. The details are given below.

II.2 Manual MART planning

We have clinically implemented manual MART planning procedure at Stanford University Hospital and over hundred breast cancer patients have been treated using the new technique. Before the implementation, several related clinical issues, including the use different types of wedges (physical or dynamic), field width problem, incorporation of MLC transmission into the step-and-shoot delivery, and QA, were extensively investigated. Our study indicated that the MART markedly improves breast irradiation and provides superior dose distributions needed to reduce radiation side effects and complications. The technique is especially valuable for radiation treatment of large-breasted women, where it is difficult to achieve homogeneous target dose distribution. The study is summarized here.

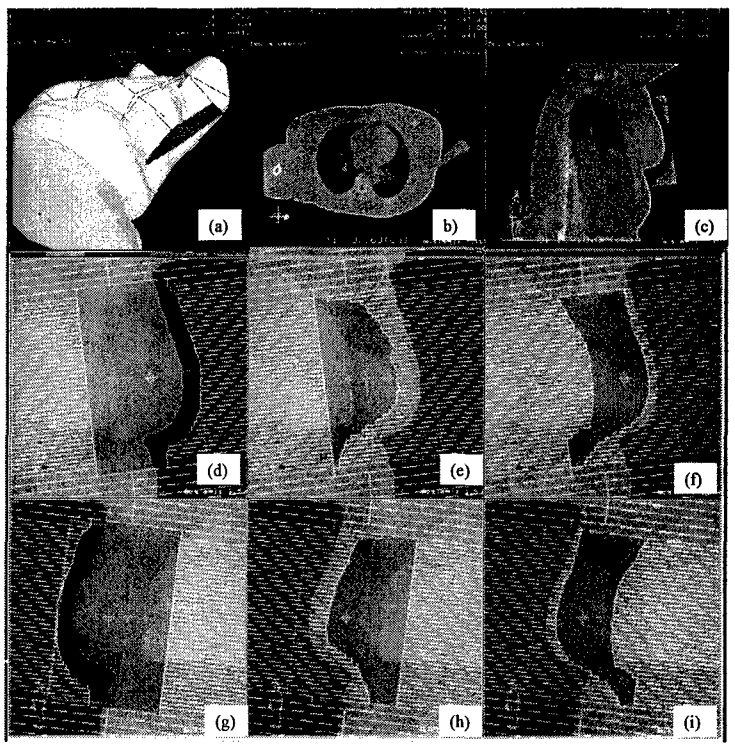

Figure 1 Standard tangential field arrangement for treatment of a left breast cancer patient (top row). The middle and bottom rows are the MLC shapes of the three segments of the medial and lateral MSRT fields, respectively. A physical wedge of 30° was used in the lateral field.

The MART patients underwent computed tomography (CT) in the conventional treatment position supported by an Alpha Cradle immobilization device (Smithers Medical Products, Tallmadge, Ohio). Radiopaque markers were placed on the patients' chest to indicate the medial and lateral borders of the palpable breast tissue and the location of the lumpectomy scar. The radiation-sensitive structures included the left and right lungs, the heart, and the contralateral breast. For the purpose of quantitative study, the contours of the skin, target volume and the sensitive structures were outlined using the segmentation tools provided by the virtual simulation workstation (AcQSim^{TM}, Philips Medical System, Cleveland, OH). It is, however, not required to outline the structures in general MART treatment. The tangential fields were determined by the routine virtual simulation procedure performed on an AcQSim workstation. The fields may be adjusted at the stage of treatment planning according to the actual treatment objective for each patient with considerations concerning tumor bed coverage, in-field lung and cardiac

volume, if left breast irradiation. Figure 1a shows an example of the OTF setup for the treatment of a left breast cancer patient. A flash region of 2 cm was used in the anterior field boarder to account for patients' respiration motion and setup uncertainty.

Manual treatment planning was done with a 3D treatment planning system (FOCUS^{TM}, Computerized Medical System, St. Louis, MO). For comparison, two plans were generated for each patient in the study. One was the standard OTF plan and the other one was the MART plan. Standard plan involved a medial and lateral tangential field with 6 or 15 MV photon energy. A wedge filter was used in the lateral direction. When a physical wedge was used, we avoided placing it in the medial field to reduce the scatter dose to the lung/heart and the contra-lateral breast. In this case, both fields were modulated with multiple segments. The segmented fields in the lateral direction were delivered concurrently with the physical wedge in place. All plans were obtained through manual trial-and-error process.

The MART planning started with a standard OTF plan. After this, we proceeded to introduce an additional MLC field segment to one or both beam directions to boost the "cold" region(s) under the guidance of dose distributions in the plane perpendicular to the incident beam direction. Figures 1d-1i show the three segments of the lateral and the medial fields for a MART treatment. The weights and MLC apertures of the segments were adjusted manually to achieve a uniform dose distribution. Our experience indicated that, for intermediately complex cases, it was often sufficient to introduce one or two additional segments to the original opposed tangential fields. For complex cases, two or three additional segments were frequently used. A segment with ipsilateral lung or heart blocked by MLC (the third segment in either medial or lateral MART field) was also helpful in reducing the dose to these structures.

The above procedure also applies to the dynamic wedge-based breast irradiation. A complication with dynamic wedge based MART arises from the interplay between the MLC leaf movement and the dynamic jaw motion when the two means of beam modulations are employed simultaneously. In reality, there are two ways to proceed. The first one is to plan the treatment using the above MART scheme and then deliver the segmented MLC fields and the dynamic wedge field separately. The major disadvantage of this approach is that it doubles the number of delivery fields and prolongs the treatment. To facilitate the treatment, we can restrict one of the incident beam to be modulated with only dynamic wedge and the other beam with only MLC-shaped segmented fields. This approach enabled us to take advantage of the MSRT treatment yet avoiding the separated delivery of the dynamic wedge field and the multiple segmented fields.

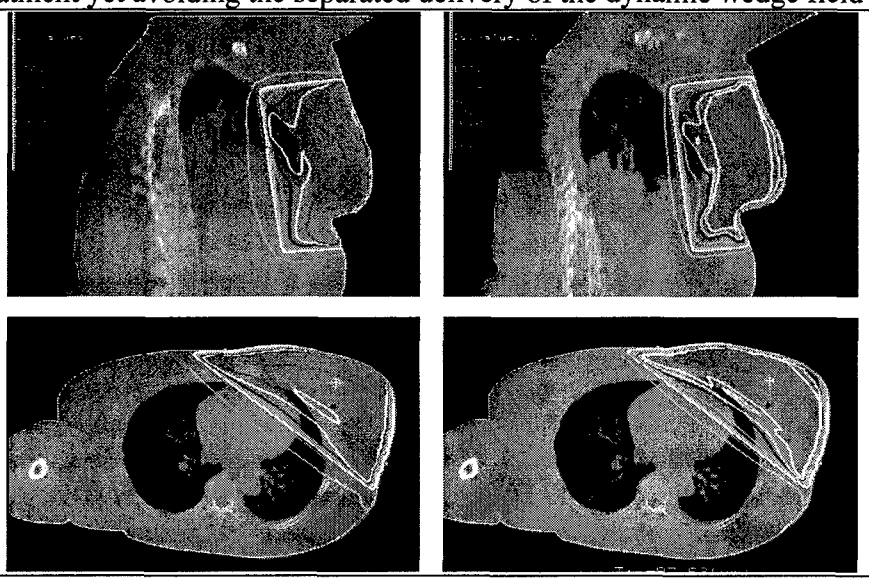

Figure 2. Comparison of the isodose distributions of the treatment plans of the left-sided breast case using the tangential field technique (a), MART (b). Target volume includes the whole breast and the internal mammary nodes. Isodose levels are shown at 110%, 100%, 90%, 70%, 50%, 30%, and 10%.

In Table 1 we summarize the treatment plans obtained using the standard OTF technique and MART. Minimum, maximum, and mean doses in the breast target volume and critical structures are given for each treatment plan. For these cases, the prescribed dose was specified to a point ~3 cm anterior to the isocenter and it was desired that the 100% isodose curve to cover the breast target volume. For comparison, we have scaled the prescription dose of all treatment plans to 5,040 cGy. The hot spots of the standard OTF plans in

the breast volume ranged from 109% to 118% when normalized to the prescription dose. These plans represented typical clinical cases that fell into the category of intermediately complicated or complicated cases. The isodose distributions in the central transverse section and in a plane perpendicular to the incident beams for the standard OTF and MART treatments are plotted in figure 2. It is seen that the dose inhomogeneity in the target volume was significantly reduced with MART, as well as reduction in the high dose to the ipsilateral lung and heart when compared with the OTF plan. The target maximum dose was reduced from 118% to 112% for the MART plan. Furthermore, the target volume receiving high dose irradiation was significantly reduced. In order to include the medial breast tissue into the radiation field, ~10% of the heart volume and the left lung were included in the tangential fields. As thus, a significant fraction of the heart and lung receives high radiation dose in standard OTF plan. The high doses to the heart was reduced by almost 6% using MART technique as a result of adding one additional segment in each incident beam (figures 1f and 1i), together with ~5% improvement in the maximum target dose in the target volume. The heart volume and ipsilateral lung volumes receiving high dose irradiation were also markedly reduced for MART treatment.

Table 1: Doses for ten breast cases. Five left breasts (#1-5) and five right breasts (#6-10) were studied. Results of two different treatment techniques (standard OTF and MART) are listed here. The breast size is defined by the dimension of the medial field (the first number is the inferior-superior dimension and the 2nd one measures the distance in the posterior-anterior direction), and the distance between the entrance points of the medial and the lateral fields.

Patient	Breast size	Standard plan					MART				
#	(cm^3)	D^T_{max}	D^T_{min}	D^T_{ave}	D^L_{max}	D^H_{max}	D^T_{max}	D^T_{min}	D^T_{ave}	D^L_{max}	D^H_{max}
1	13.0x20.6x26.7	5932	3235	5212	5494	5312	5653	3247	5240	5342	4989
2	9.5x22.0.x19.1	5692	3497	5155	5314	4501	5536	3465	5111	5232	4140
3	14.0x19.0x24.1	5861	3593	5236	5363	4658	5630	3579	5117	5122	4452
4	8.0x16.5x17.7	5513	3738	5028	4867	4408	5369	3783	5047	4847	4427
5	10.0x19.2x16.8	5686	4497	4886	5467	4908	5421	4639	4792	5203	4824
6	9.0x20.0x21.1	5703	3940	5230	5101	*	5532	3939	5195	5015	*
7	8.0x18.2x17.0	5590	4066	5111	5172	*	5408	4053	5082	5099	*
8	7.0x14.0x17.9	5630	4175	5113	5542	*	5433	4125	5043	5345	*
9	8.5x19.0x19.0	5838	4027	5185	5257	*	5471	4005	5120	5207	*
10	9.0x17.5x20.2	5799	3823	5217	5424	*	5535	3808	5148	5268	*

The MLC movement trajectories (or leaf sequences) were known upon the completion of MART plan and there was no need for a leaf sequencing algorithm to convert an optimal fluence map into MLC sequences. The static MLC file of each segment was exported as an ASCII file from the FOCUS treatment planning system. For each gantry angle, the segmented fields were stacked together to form a step-and-shoot delivery using a simple software tool, developed in-house, which reads in each individual MLC segment and exports the step-and-shoot delivery file according to the MLC manufacturer's specifications of the file structure. In addition, a step-and-shoot delivery file for portal verification was also generated. The step-and-shoot files must have correct CRC (computer redundancy check) code attached at the end of the file in order to be executable by the MLC workstation.

II.3 Improve IMRT/MART dose distribution by using spatially non-uniform importance factors

We are developing an effective aperture based optimization algorithm for breast irradiation. In current inverse planning algorithms it is common to treat all voxels within a target or sensitive structure equally and use structure specific prescriptions and weighting factors as system parameters. In reality, the voxels within a structure are not identical in complying with their dosiemtric goals and there exists strong intra-structural competition in these voxels. Inverse planning objective function should not only balance the competing

objectives of different structures but also that of the individual voxels within various structures. We have proposed an approach to improve IMRT treatment plan by purposely modulating the penalty on individual voxel level based on the *a priori* dosimetric capability information of the dose optimization system. We quantify the degree for a voxel to achieve its dosimetric goal by introducing the concept of dosimetric capability for each voxel in a target or sensitive structure and describe a Cimmino algorithm for numerically computing the capability distribution on a case specific basis. The capability of a voxel represents *a priori* dosimetric knowledge of the system and is useful to construct an objective function with customized non-uniform importance factors. A general inverse planning framework with customized non-uniform importance factors has been established. It has been shown that the incorporation of the capability information permits us to construct physically and clinically more meaningful objective function and greatly enlarge the universe of solution space, leading to significantly improved MART/IMRT treatment plans that would otherwise unattainable. Figure 3 shows a comparison of MART/IMRT phantom plans obtained with and without using spatially non-uniform penalty and it is seen that, by purposely modulating the spatial penalty, the dose to the sensitive structure is remarkably reduced by almost ~18% (normalized to the maximum sensitive structure dose) everywhere. In this case, the dose everywhere within the sensitive structure was reduced by ~17%. Clinically, this also implies that the target dose may be escalated by ~10% while keeping the toxicity at the level achievable by current IMRT planning technique. Considering the improvement was accomplished purely from a more physical modeling of the system, the result is quite striking. Our results reveal that the MART/IMRT plans obtained using structurally uniform importance factors (current practice) are, at best, sub-optimal and there is an urgent need for a systematic approach to deriving the patient specific local importance distribution to improve the current inverse planning techniques. The underlying principle here is to adjust the local importance to effectively "boost" those regions where there are problems in meeting their dosimetric goals. This work has recently been submitted to Physics in Medicine and Biology for consideration of publication. The new penalty scheme is being implemented in our MART optimization development [15].

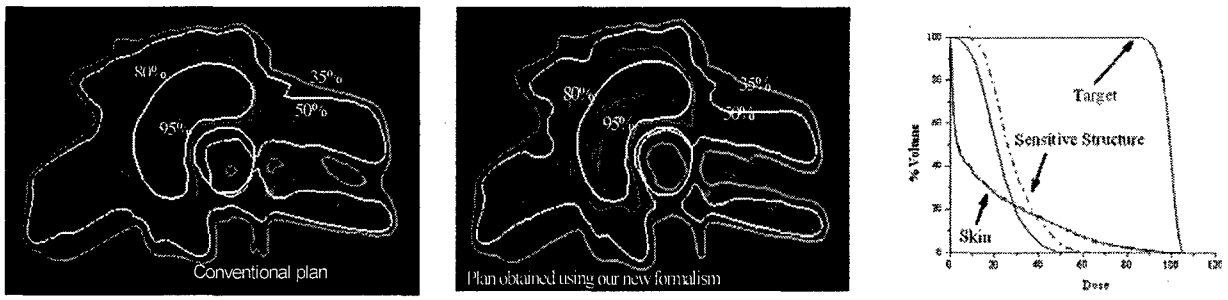

Fig. 3 IMRT plans for a hypothetical test case: (left) uniform importance (conventional scheme); (middle) non-uniform importance for both target and sensitive structure. Half-moon shaped white structure is the target and the circular while structure close to target is the sensitive structure to spare. Red, pink, yellow, and blue curves represent 95%, 80%, 50%, and 35% isodose curves. A comparison of DVHs is shown in the right panel. The dashed and solid curves correspond to the IMRT plans with uniform and non-uniform importance distributions, respectively.

III. KEY RESEARCH ACCOMPLISHMENTS

- Developed a manual MART planning procedure and assessed the dosimetric improvement resulted from MART.
- Demonstrated the advantage of MART over conventional OTF plans;
- Clinically implemented MART treatment technique and over hundred breast cancer patients have been treated using the new technique.
- Developed a software tool that concatenates multiple segments for step-and-shoot delivery with incorporation of MLC transmission and head scatter into MLC leaf sequencing process, which makes it possible to accurate deliver the optimal treatment plans.

- Constructed a dosimetric phantom that is capable of simulating the patient's breathing motion. The dosimetric influence of the breathing motion is being carried out using the phantom.
- Improved current inverse planning framework by introducing a voxel dependent penalty scheme and demonstrated its superiority.

IV. REPORTABLE OUTCOMES

The following is a list of publications resulted from the grant support. Copies of the publication materials are enclosed with this report.

Refereed publication:

- **Shou Z,** Yang Y, Cotrutz **C** and Xing L, Quantitation of the *a priori* dosimetric capabilities of spatial points in inverse planning and its significant implication in defining IMRT solution space. Submitted to *Physics in Medicine and Biology.*

Published Abstracts:

The PI's group has also been active in disseminating our research results. The following are some of the presentations given in various national/international meetings.

- Lo A, **Shou Z** and Xing L, Quantitative comparison of aperture-based and beamlet-based inverse planning techniques, *International Journal of Radiation Oncology, Biology, Physics, Volume 60, 1, Supplement 1, September 2004, Pages S630-S630;*
- **Shou Z** and Xing L, Aperture-based IMRT inverse planning with incorporation of organ motion, *International Journal of Radiation Oncology, Biology, Physics, Volume 60, 1, Supplement 1, September 2004, Pages S631-S632.*
- Xing Land **Shou Z,** Intrinsic spatial heterogeneity in inverse planning and its significant role in defining the universe of IMRT solution space, *International Journal of Radiation Oncology, Biology, Physics, Volume 60, 1, Supplement 1, September 2004, Pages S635-S635.*
- **Shou Z** and Xing L: Improve IMRT distribution by using spatially non-uniform important factors, oral presentation in 2004 annual meeting of ICCR in Seoul, Korea. 120-123, 2004.
- Xing L, Hunjan S, Lian J, Yang Y, **Shou Z,** Schreibmann E, Boyer A, Towards Biologically Conformal Radiation Therapy: Functional and Molecular Image Guided Intensity Modulated Radiation Therapy, XIVth International Conference on the Use of Computers in Radiation Therapy (ICCR), Soul, Korea, 2004.

V. CONCLUSIONS

Despite the well-appreciated fact that intensity-modulation could lead to significantly improved dose distributions in breast irradiation, its clinical implementation has been hindered by the deficiencies in the current inverse planning system and by the lack of a comprehensive treatment procedure. This is evidenced by the fact that very few institutions are using IMRT routinely for breast cancer treatment. A clinical challenge in IMRT breast treatment is how to modulate breast irradiation without increasing the treatment complexity. In this work, the utility of MART for breast irradiation has been evaluated. Two different delivery schemes with physical wedge or dynamic wedge have been discussed to meet the requirements of different clinical environments. It was found that, with the use of MART technique, high doses to the ipsilateral lung and, in the case of the left-breast cancer patient, the heart were reduced and the dose

homogeneity in the breast target volume was significantly improved by using the technique. The new treatment scheme is especially valuable for treating patients with large-sized breasts. A novel voxel dependent penalty scheme was proposed to improve the currently existing dose optimization scheme. In addition, technique of incorporating MLC transmission and head scatter has been developed to ensure that the accuracy of MART delivery. The manual MART planning and treatment has been implemented in Stanford University Hospital and it is now part of standard practice here.

References

1. Fisher B, Redmond C, Poisson R, et al.: Eight-year results of a randomized clinical trial comparing total mastectomy and lumpectomy with or without irradiation in the treatment of breast cancer. New England Journal of Medicine 1989; 320(13): 822-8.
2. Fisher B, Costantino J, Redmond C, et al.: Lumpectomy compared with lumpectomy and radiation therapy for the treatment of intraductal breast cancer. New England Journal of Medicine 1993; 328(22): 1581-6.
3. Dobbs HJ: Radiation therapy for breast cancer at the millennium. Radiotherapy & Oncology 2000; 54: 191-200.
4. Asrari F, Gage I: Radiation therapy in management of breast cancer. Current Opinion in Oncology 1999; 11(6): 463-7.
5. Arbetter KR, Prakash UB, Tazelaar HD, Douglas WW: Radiation-induced pneumonitis in the "nonirradiated" lung. Mayo Clinic Proceedings 1999; 74(1): 27-36.
6. Shapiro CL, Hardenbergh PH, Gelman R, et al.: Cardiac effects of adjuvant doxorubicin and radiation therapy in breast cancer patients. Journal of Clinical Oncology 1998; 16(11): 3493-501.
7. Rutqvist LE, Lax I, Fornander T, Johansson H: Cardiovascular mortality in a randomized trial of adjuvant radiation therapy versus surgery alone in primary breast cancer [see comments]. Comment in: Int J Radiat Oncol Biol Phys 1992;22(5):1157-8. International Journal of Radiation Oncology, Biology, Physics 1992; 22(5): 887-96.
8. Rothwell RI, Kelly SA, Joslin CA: Radiation pneumonitis in patients treated for breast cancer. Radiotherapy & Oncology 1985; 4(1): 9-14.
9. Karlsson M, Zackrisson B: Matching of electron and photon beams with a multi-leaf collimator. Radiotherapy & Oncology 1993; 29(3): 317-26.
10. Li JG, Williams SS, Goffinet DR, Boyer A, Xing L: Breast-conserving radiation therapy using combined electron and IMRT technique. Radiotherapy & Oncology 2000; 56: 65-71.
11. Smitt MC, Li SD, Shostak CA, Chang W, Boyer AL: Breast-conserving radiation therapy: potential of inverse planning with intensity modulation. Radiology 1997; 203(3): 871-6.
12. Hong L, Hunt M, Chui C, et al.: Intensity-modulated tangential beam irradiation of the intact breast. International Journal of Radiation Oncology, Biology, Physics 1999; 44(5): 1155-64.
13. Kestin LL, Sharpe MB, Franzier RC, et al.: Intensity-modulation to improve dose uniformity with tangential breast radiotherapy: initial clinical experience. International Journal of Radiation Oncology, Biology, Physics 2000; 48: 1559-1568.
14. Lo YC, Yasuda G, Fitzgerald TJ, Urie MM: Intensity modulation for breast treatment using static multi-leaf collimators. International Journal of Radiation Oncology, Biology, Physics 2000; 46(1): 187-94.
15. Shou Z and Xing L, Aperture-based IMRT inverse planning with incorporation of organ motion, *International Journal of Radiation Oncology, Biology, Physics, Volume 60, 1, Supplement 1, September 2004, Pages S631-S632.*

Appendix I. Copy of a manuscript

Quantitation of the *a priori* dosimetric capabilities of spatial points in inverse planning and its significant implication in defining IMRT solution space

Zhenyu Shou, Yong Yang, Cristian Cotrutz, and Lei Xing

Department of Radiation Oncology, Stanford University School of Medicine,

875 Blake Wilbur Drive, Stanford, California, CA 94305-5847

Corresponding author:
Lei Xing, Ph.D.
Stanford University School of Medicine
Department of Radiation Oncology
875 Blake Wilbur Drive
Stanford, CA 94305-5304

E-mail: lei@reyes.stanford.edu
Phone: (650) 498 7896
Fax: (650) 498 4015

Purpose: In this work we propose an approach to quantify the *a priori* dosimetric capability for a spatial point to meet its dosimetric goal in dose optimization system and show its significant role in improving IMRT treatment plans.

Methods and Materials: We quantify the degree for a voxel to achieve its dosimetric goal by introducing the concept of dosimetric capability for each voxel in a target or sensitive structure, and describe a Cimmino algorithm for numerically computing the capability distribution on a case specific basis. The capability of a voxel represents the *a priori* dosimetric knowledge of the system and is useful in constructing an objective function with customized non-uniform importance factors. Generally speaking, the final optimal dose distribution depends not only on the prescription and the values of the structure specific importance factors, but also on the dosimetric capability distribution in an implicit fashion. In some extreme cases, a region in a target may never meet the prescribed dose without seriously deteriorating the doses in other areas. Conversely, the prescription in a region may be easily met without violating the tolerance of any sensitive structure. The intra-organ tradeoff was modulated purposely using a heuristic model with consideration of the heterogeneity of the dosimetric capability of the system. The formalism is applied to a few specific examples to illustrate the technical details of the new inverse planning technique.

Results: The dosimetric capability of a voxel has been proved to be a useful measure of the relative ease for a point in the target or sensitive structure to achieve its dosimetric goal. An inverse planning framework with customized non-uniform importance factors has been established. It has been shown that the incorporation of the capability information permits us to construct a physically and clinically more meaningful objective function and greatly enlarge the solution space. The modulation of the spatial penalty distribution has been shown to be advantageous over the conventional inverse planning technique with structurally uniform importance factors, leading to significantly improved IMRT treatment plans that would otherwise be unattainable.

Conclusion: Knowing the *a priori* capability distribution of the system sheds new insight into the inverse planning problem and allows us to better interpret a patient's IMRT dose distribution. The tacit assumption in current inverse planning that all points within a structure are equivalent represents only one of numerous penalty schemes (generally, not an optimal one) and IMRT dose optimization can be improved by incorporating the *a priori* dosimetric capability information.

Key Words: IMRT, inverse planning, dose optimization, treatment planning, prior knowledge.

INTRODUCTION

The inverse planning method is usually used to obtain IMRT treatment plans. A tacit assumption made in current inverse planning algorithms is that all points within a structure are equivalent. In these algorithms, the dose prescription, weighting factors and dose-volume constraints are generally imposed *a priori* on a structure specific basis without clearly knowing their consequences on the final solution. (Bortfeld et al 1990, Brahme et al 1982, Cho et al 1998, Gopa and Starkschall 2001, Holes and Mackie 1994, Langer and Leong 1987, Spirou and Chui 1998, Webb 1991, Zagars et al 2002). Even in the recently proposed EUD-based inverse planning scheme (Wu et al, 2002, Thieke et al 2003, Lian and Xing 2004), this remains unchanged since no voxel-dependent information is involved in specifying an EUD prescription and the parameter n, which plays the role of weighting factor as in the conventional dose optimization scheme. In reality, voxels within a structure are generally not equivalent in achieving their dosimetric goals. The level of ease for a point to meet its dosimetric goal depends not only on the importance factor of the structure and the deviation of the dose at the point from the prescribed value, but also the spatial location of the point relative to the beams and patient geometry because of the intrinsic spatial heterogeneity of the system (Cotrutz and Xing 2002, 2003, Wu et al 2003). To conceive this, it may be useful to imagine a simple situation where a beam incidents perpendicularly into a cubic phantom. In this particular case, the desire of uniformly irradiating the points inside the beam is clearly unrealizable and a prescription dose can only be met at one depth. In general, depending on the patient's geometry, beam modality and field configuration, some regions in a patient may have better chance to meet the prescription than others, and *vice versa*. This type of information represents *a priori* knowledge of a given system and the inclusion of the knowledge should facilitate the search for a truly optimal solution in IMRT plan optimization.

The purpose of this work is to establish a general framework for incorporating *a priori* voxel-dependent capability information into inverse planning and to demonstrate the utility of the new formalism. To this end, we will introduce the concept of dosimetric capability for an arbitrary voxel in a target or sensitive structure and use it to quantify the level of ease for the voxel to meet the specified dose. A voxel dependent penalty scheme, in which the penalty at a voxel depends not only on the dose deviation from the prescription but also on the physical limitation at the point, is then constructed by lifting the restriction of uniform importance factors for the involved structures. Ideally, one can treat these voxel-dependent importance factors as part of the system parameters and optimize them along with the beamlet weights (Chen et al 2002, Wu and Zhu 2001, Xing et al 1999). While this does not

pose any conceptual challenge, the search space becomes enormous due to the coupling between beamlet weights and the local importance, and the vast amount of computing time required for this type of calculation renders it impractical for clinical or even research application. The heuristic approach developed in this work allows us to circumvent the problem to effectively estimate the local importance factor distribution based on the capability calculation. It seems that the technique captures the main feature of the modeling of intra-organ tradeoff and thus is capable of generating superior IMRT treatment plans. Application of the new technique to a few cases suggests that the dose distributions obtained with conventional inverse planning algorithm based on structurally uniform importance factors are at best sub-optimal and can be significantly improved with the help of the proposed non-uniform penalty scheme.

METHODS AND MATERIALS

Theoretical background

The three dimensional patient volume is divided into a grid of N total voxels for dose calculation. Each incoming beam is modeled by a two dimensional fluence function, which is discretized into M beamlets of 1cm x 1cm. A beamlet (or a pixel) of a fluence map is indexed by (j,m), where j and m are the indices of the beam and the beamlet in the beam, respectively. The dose is computed according

$$D_c(n_\sigma) = \sum_{jm} d_{jm}(n_\sigma) w_{jm}, \qquad (1)$$

where $d_{jm}(n_\sigma)$ is the dose kernel that represents the dose contribution to voxel n_σ from the beamlet (j,m) and w_{jm} is the weight of the beamlet. For each voxel, the contribution to the dose primarily comes from a limited number of beamlets that directly traverse across the voxel. Other beamlets contribute to the dose at the voxel through scatter.

Given a prescription, the task of inverse treatment planning is to derive the optimal beam profiles (or the weights of all beamlets) that produce a conformal dose distribution as close as possible to the prescription. The search for the optimal solution is guided by an objective function, which is a measure of the goodness of a physically realizable solution. To be specific, in this work we use a generalized quadratic objective function defined by

$$F = \sum_{\sigma} \sum_{n_\sigma=1}^{N_\sigma} \frac{r_\sigma r_{n_\sigma}}{N_\sigma} (D_c(n_\sigma) - D_\sigma^{pre})^2 \quad , \qquad (2)$$

where r_σ and r_{n_σ} parameterize the inter-structural and intra-structural tradeoffs, respectively, and N_σ is the total number of voxels in the σ-th structure. $D_c(n_\sigma)$ is the actual dose delivered to voxel n_σ and D_σ^{pre} the prescribed dose. For a sensitive structure, we set $D_\sigma^{pre} \equiv 0$ so that the doses to the normal tissue voxels are continuously decreased when there is room for improvement, instead of being "forced" to receive the tolerance dose. The objective function as defined in (2) is the same as the commonly used quadratic objective function (Bedford et al 2002, Bortfeld 1990, Das et al 2003, Langer et al 1990, Webb et al 1998, Xing and Chen 1996, Michalski et al 2004). When $r_{n_\sigma} \equiv 1$, in which case the voxels in an involved structure become equivalent and have the same importance during the dose optimization. The conventional penalty scheme seriously limits the solution space and often leads to a sub-optimal plan. To give a comprehensive example, one can imagine the consequence when two or more structures in a system are restricted to take a single importance value. The penalty function defined in Eq. (2) provides a natural way to formalize a voxel dependent penalty scheme and allows us to access more candidate plans. The local or voxel dependent importance factor has been used previously to manually "tweak" the regional doses upon completion of a conventional dose optimization (Cotrutz and Xing 2002, 2003, Wu et al 2003). It will be seen later that the determination of $\{ r_{n_\sigma} \}$ distribution can be facilitated by the use of *a priori* dosimetric capability information of the system.

Definition of dosimetric capability

The likelihood for a voxel to meet its dosimetric goal can be quantified by introducing the concept of dosimetric capability. For illustration purposes let us first assume that there is only one incident beam. For a target voxel, the capability is assessed by the degree to which the voxel meets the prescription without violating the tolerance of the sensitive structure. The maximum achievable dose, $D^{ach}(n_\sigma)$, at the voxel n_σ in the target is determined by scaling the intensity of the contributing beamlet to the highest value set by the tolerance of the sensitive structure. Mathematically, the "capability", η, is defined as

$$\eta(n_\sigma) = \frac{D^{ach}(n_\sigma)}{D_\sigma^{pre}} \quad . \qquad (3)$$

The evaluation of Eq. (3) is straightforward for the case of a single incident beam or when there is no overlap of beamlets at the dose limiting voxel in the sensitive structure. For multi-field IMRT, the $D^{ach}(n_\sigma)$ is determined not only by those beamlets that directly intercept the voxel *n*, but possibly other beamlets irradiating different parts of the target. The coupled system can be described by a set of linear equations (which can be easily written down from Eq. (1) and the above definition of the maximum achievable dose). The $D^{ach}(n_\sigma)$ of a target voxel will be obtained by optimizing the linear system, under the condition that the total dose at an arbitrary sensitive structure voxel is equal to its tolerance dose. The beam profiles so obtained deliver the maximum dose to the target without violating the tolerances of the sensitive structures. Mathematically, the system equations are underdetermined and a Cimmino algorithm can be used to find the solution Starkschall and Eifel 1992, Xiao et al 2000). The calculation consists of the following steps:

(i) Assign all beamlets with high enough initial intensities (say, two or three times the intensity values that deliver the prescribed dose the to the target);

(ii) Compute the dose distribution using Eq. (1);

(iii) (a) Choose a beamlet in a beam and locate the voxels in sensitive structures that are traversed by the beamlet;

(b) For each located voxel in the sensitive structures, check if the tolerance is exceeded. If yes, decrease the value of the beamlet based on a Cimmino algorithm described in more details later;

(c) Update the dose;

(d) Repeat step (b) and (c) until all voxels intercepted by the beamlet are checked.

(iv) Repeat from (ii) until the doses in sensitive structures are equal to their tolerances.

The above beamlet-by-beamlet updating scheme is similar to the simultaneous iterative inverse planning technique (SIITP) (Xing and Chen 1996). However, the goal here is not to find the optimal IMRT solution, but, instead, to search for the beam profiles that deliver the highest achievable doses in the target, $D^{ach}(n_\sigma)$, without violating the dose tolerance of the involved sensitive structures (in other words, any increase in the beamlet weights would lead to a dose exceeding the tolerance in one or multiple points inside a sensitive structure). Mathematically, the algorithm falls into the realm of the Cimmino feasibility algorithm, which is an iterative projection

algorithm converging to a feasible solution if the constraints are satisfied, otherwise to a compromise solution that minimizes the weighted sum of squares of deviations from the tolerance doses if dose constraints are violated. The beamlet weights in the Cimmino algorithm are updated according to

$$w_{jm}^{k+1} = w_{jm}^{k} + \lambda \sum_{n_\sigma} z_{n_\sigma} c_{n_\sigma}(w^k) d_{jm}(n_\sigma), \qquad (4)$$

where

$$c_{n_\sigma}(I^k) = \begin{cases} \dfrac{(D_\sigma^{pre} - D_c^k(n_\sigma))}{\sum_{jm} d_{jm}^2(n_\sigma)} & \text{if} \quad D_c^k(n_\sigma) > D_\sigma^{tol} \text{ and } n_\sigma \in \text{sensitive structures} \\ 0 & \text{otherwise,} \end{cases}$$

and $z_{n_\sigma} > 0$. Note that in the conventional Cimmino algorithm, the values of z_{n_σ} are constrained by $\sum_{n_\sigma} z_{n_\sigma} = 1$. In our calculation, the algorithm is over-relaxed by simply setting

$$z_{n_\sigma} \equiv \frac{r_\sigma r_{n_\sigma}}{N_\sigma} \quad ,$$

which is the product of the structural and intra-structural weighing factors. The relaxation parameter λ is generally set to a small value ($0.02 < \lambda < 0.1$) to ensure a smooth updating of the beamlet weights. We found that these modifications resulted in an improved convergence. The merit of the updating scheme can be evaluated at each iteration step by a proximity function constructed from the weighted sum of squares of dose deviations of the voxels violating the dose limit constraints[18]

$$F = \sum_{n_\sigma \in \text{sensitive structure}} \frac{r_\sigma r_{n_\sigma}}{N_\sigma} [(D_c(n_\sigma) - D_\sigma^{tol})^+]^2 \quad , \qquad (5)$$

where $x^+ \equiv \max(0, x)$.

The calculation described above can be similarly done for sensitive structures. The dosimetric capability of a voxel in a sensitive structure is characterized by the minimum achievable dose at the voxel needed in order to administer the prescribed dose to the target voxels. For consistency, we denote the minimum achievable dose by $D^{ach}(n_\sigma)$ (where n_σ represents a voxel in the sensitive structure) and quantify the dosimetric capability of the voxel according to

$$\eta(n_\sigma) = \frac{D_\sigma^{tol}}{D^{ach}(n_\sigma)} \quad . \qquad (6)$$

For a voxel in a sensitive structure, the lower the minimum achievable dose, the more "capable" the voxel is. The evaluation of Eq. (6) is once again straightforward for the case with a single incident

beam. To obtain the minimum achievable dose, one can first set the corresponding beamlet to such an intensity that the prescribed dose is delivered to the target voxels, and then evaluate the dose, $D^{ach}(n_\sigma)$, at n_σ in the sensitive structure. To obtain the capability map when there are multiple incident beams, a set of linear equations (which can be easily written down from Eq. (1) and the above definition of the minimum achievable dose) need to be solved under the condition that the target voxels receive their prescription doses. Similar to the target case, the system equations become undertermined when there are multiple incident beams and a Cimmino algorithm is used to find the beam profiles that yield the lowest achievable dose in the sensitive structures. For convenience, the calculation procedure for a sensitive structure voxel is outlined as follows.

(i) Assign all beamlets with low enough initial intensities so that doses delivered to the target voxels are less than the prescription;

(ii) Compute the dose distribution using Eq. (1);

(iii) (a) Choose a beamlet in a beam and locate the voxels in the target that are traversed by the beamlet;

(b) For each located voxel in the target, check if the dose prescription is exceeded. If yes, lower the beamlet weight based on a Cimmino algorithm outlined later;

(c) Update the doses;

(d) Repeat step (b) and (d) until all voxels intercepted by the beamlet are checked.

(iv) Repeat from (ii) until the doses in target voxels meet the prescription.

We update the beamlet weights as follows

$$w_{jm}^{k+1} = w_{jm}^{k} + \lambda \sum_{n_\sigma} z_{n_\sigma} c_{n_\sigma}(w^k) d_{jm}(n_\sigma) , \qquad (7)$$

where

$$c_{n_\sigma}(w^k) = \begin{cases} \dfrac{(D_\sigma^{pre} - D_c^k(n_\sigma))}{\sum_{jm} d_{jm}^2(n_\sigma)} & \text{if} \quad D_c^k(n_\sigma) < D_\sigma^{pre} \text{ and } n_\sigma \in \text{target} \\ 0 & \text{otherwise.} \end{cases}$$

The corresponding proximity function now becomes

$$F = \sum_{n_\sigma \in target} \frac{r_\sigma r_{n_\sigma}}{N_\sigma} [(D_\sigma^{pre} - D_c(n_\sigma))^+]^2 \ . \qquad (8)$$

We emphasize that the beam profiles obtained above are not intended to approximate the optimal fluence profiles for IMRT treatment. Instead, they are obtained purely for the purpose of evaluating the dosimetric capabilities of voxels in a target or a sensitive structure. Once the capability maps are obtained, they can be incorporated into an inverse planning procedure to yield clinically more advantageous plans. This is the subject of the following section.

Incorporating dosimetric capability into inverse planning

In conventional IMRT inverse planning, a uniform importance factor is usually assigned to each involved structure (Cho et al 1998, Holmes and Mackie 1994, Oelfke and Bortfeld 1999, Olivera et al 1998), which seriously limits the solution space. To give a comprehensive example, one can imagine the consequence when two or more structures in a system are restricted to take a single importance. To be able to assess more candidate plans, it is necessary to establish a voxel dependent penalty scheme in which the penalty at a voxel depends not only on the dose deviation from the prescription but also on the physical and clinical requirements at the point. A natural way to achieve this is to lift the restriction of uniform importance for a structure so that the importance at a voxel can be adjusted independently. The commonly used penalty scheme with uniform importance factor is simply a special case of the general penalty scheme. While conceptually being acceptable, a practical question is how to determine the optimal importance distribution within a structure. In the following, we heuristically relate the local importance to the capability derived earlier and use this relation as a means to obtain an adequate importance factor distribution.

The capability distribution contains information about the intrinsic heterogeneity of the dosimetric capability and reveals which points are likely to violate/conform the prescription. The data can be used to heuristically estimate the local importance distribution. While it is not difficult to intuitively conceive the general behavior of the relation between local importance and the capability, its specific form is a matter of experimenting. The relation between the local importance and the capability used in our study is

$$\tilde{r}(n_\sigma) = (1 + g(n_\sigma)^\alpha) r_\sigma, \qquad (9)$$

where α is a positive constant and $g(n_\sigma)$ is empirically defined as

$$g(n_\sigma)=\begin{cases}\dfrac{r_{max}}{\left(\eta_\sigma^{max}-1\right)}\left(\eta(n_\sigma)-1\right) & n_\sigma \in \text{target} \quad \text{and} \quad \eta(n_\sigma)\geq 1 \\ \dfrac{r_{max}}{\left(\eta_\sigma^{min}-1\right)}\left(\eta(n_\sigma)-1\right) & n_\sigma \in \text{target or sensitive structure} \quad \text{and} \quad \eta(n_\sigma)<1\end{cases} \tag{10}$$

The capability map and the corresponding η_σ^{max} or η_σ^{min} is obtained for each structure. In Eq. (10), we typically choose $\alpha=2$ and $r_{max}=3$. For a sensitive structure, if $\eta(n_\sigma)>1$, it means that the voxel has no difficulty meeting its dosimetric goal and $g(n_\sigma)$ is set to zero. The basic strategy is to assign a higher penalty (or high importance) to those voxels with lower capabilities (those voxels are likely to have a dose lower than the prescription if they are in the target volume, or higher than the tolerance if they are located in a sensitive structure). The differential penalty scheme allows the system to suppress potential hot spots in the sensitive structures and boost the potential cold spots in the target volume so that a more uniform dose distribution can be achieved in the target while sparing more sensitive structures, possibly leading to a solution that is more consistent with our clinical expectation.

Implementation

We implemented a software module to optimize the objective function (5) in the platform of the PLUNC treatment planning system (an open source treatment planning system from the University of North Carolina, Chapel Hill, NC). The dose calculation engine and varieties of plan evaluation tools of the PLUNC system were used to evaluate and compare the optimization results. The final IMRT plan was obtained in a similar manner as in conventional inverse planning except that the uniform importance for the involved structures are replaced by the non-uniform importance distributions given by Eqs. (9) and (10). The ray-by-ray iterative algorithm (SIITP) reported earlier [3] was employed to obtain the optimal beam intensity profiles. The calculation was performed on a PC with P4 1.7GHz and 1024MB RAM.

Test of the new dose optimization formalism

To better understand the physics behind the capability calculation, we first constructed a hypothetical surrogate case (figure 1) and studied the behavior of the system using a single beam and five incident beams. The gantry angle used for target irradiation in the single beam case was

320°, and in the five-beam case the angles used were 32°, 104°, 176°, 248° and 320°, where IEC convention for gantry angle is used. The incident photon energy was 15 MV. In both cases, the target was prescribed to 100 (arbitrary unit) and the sensitive structure tolerance was set to be 25. An IMRT treatment was also planned with the same five-beam configuration but structurally uniform importance factors and the result was compared with the newly obtained plan.

The new algorithm was also applied to two clinical cases: a prostate case and a paraspinal tumor treatment. To illustrate the advantage of the technique, the results were compared with those obtained using the conventional inverse planning with uniform importance factors. For the prostate IMRT case, six equally spaced beams starting from zero degrees were used. Some relevant parameters used for planning the patient are summarized in Table I. As in conventional inverse planning, the structure specific importance factors, $\{r_\sigma\}$, were determined by trial-and-error. To assess the new technique, we planned the case using three different strategies: (i) uniform importance for the prostate target and the sensitive structures; (ii) dosimetric capability-based non-uniform importance for the prostate target and uniform importance for all sensitive structures; and (iii) dosimetric capability-based non-uniform importance for both prostate target and the sensitive structures. The three plans were compared using DVHs and isodose distribution plots.

In the paraspinal case, the sensitive structures involved include the spinal cord, liver and kidney. In this study, five 15 MV non-equally spaced coplanar beams (40°, 110°, 180°, 255°, and 325°) were used for the treatment. The structure specific importance factors and prescription/tolerances are summarized in Table 2. IMRT plans with and without importance factor modulation were obtained and quantitative comparison was performed.

RESULTS AND DISCUSSIONS

A hypothetical test case

The capability and importance distributions for both single beam and five-beam configurations are plotted in figure 1. The iso-capability and iso-importance curves are normalized to unity. For the single beam calculation (figure 1a), it is seen from the capability map (left panel) that the target region in the middle of the incident beam has lower dosimetric capability due to the restriction of the tolerance of the sensitive structure. For the points on both sides of the central target region, the dosimetric capabilities are much higher because of the absence of sensitive

structure "blocking". The capability distribution within the sensitive structure can also be intuitively interpreted. For the voxels distant from the target volume, the capability is relatively high, indicating that these voxels are less dose-limiting points in comparison with the voxels close to the target. For the single beam case, the importance map (right panel of figure 1a) is almost an inversion of the capability map.

Figure 1b shows the capability and importance distributions when five incident beams are used to irradiate the target. The calculation is fairly efficient: it took less than 6 minutes for the system to obtain the capability and importance maps. In this case, the low capability region in the middle of the target shown in figure 1a disappears and only a few isolated low capability spots show up near the edge of the target. On the other hand, the overall behavior of the capability map in the sensitive structure is not changed dramatically. The dosimetric capabilities for those points close to the target remain relatively low, which is consistent with our intuition since, relatively speaking, these points are more dose-limiting compared to the points far away from the target. The results also suggest that the boundary region between the two structures is likely to be underdosed (for target) or overdosed (for sensitive structure). In order to improve this, a non-uniform penalty scheme derived *a priori* or *a posteriori* becomes necessary. The technique described in this paper represents an example of the *a priori* method, whereas an adaptive adjustment of the local importance factor distribution would be an example of the latter. In general, the importance distribution is not a simple inversion of the capability map and depends also on the absolute values of the capabilities, as suggested by Eqs. (9) and (10). This is especially true for the target, in which we need not only to "boost" the potential cold region(s) but also to "suppress" the potential hot spot(s). The high importance in the left-middle region of the target (see the right panel of figure 1b) is a direct consequence of the stated requirement. Indeed, a careful examination of the target capability data indicated that, the region has high dosimetric capability and is thus likely to be overdosed. The assignment of higher local importance according to Eq. (9) permits us to suppress the potential overdosing *a priori*.

In figure 2 we show the IMRT plans obtained without and with modulating the spatial importance distribution. The left panel is the conventional IMRT plan with uniform importance factors assigned to both target and sensitive structure. The right panel shows the plan obtained with spatially non-uniform importance distribution plotted in right panel of figure 1b. It is clearly seen that the isodose curves in the sensitive structure are "pushed" toward the target and the dose

gradient at the tumor boundary is greatly increased. The significant improvement can also be seen in the DVH plot (figure 3). It is remarkable that, by simply modulating the spatial importance distribution, an almost uniform reduction of ~20% (normalized to the maximum sensitive structure dose) in the dose to the sensitive structure can be accomplished. If the dose to the non-sensitive structure normal tissue is not a limiting factor, the above result suggests that the target dose can be escalated by ~10% while keeping the radiation toxicity at the current IMRT level.

Six-field IMRT prostate treatment

The IMRT plans obtained using three different penalty schemes are summarized in figures 4 and 5. The isodose distributions for the three penalty schemes are shown in figure 4. In figure 5, we compare the DVHs obtained using conventional inverse planning (dotted curves--obtained using uniform importance for the prostate target and the sensitive structures) and the new technique with non-uniform importance in both target and sensitive structures (solid curves). The DVHs of the plan with non-uniform importance to the prostate target and uniform importance to the sensitive structure are shown in dash-dotted curves. The importance factors for both target and sensitive structures were constructed based on the computed capability maps using the procedure described in the Method section. It is seen from figure 4 that the dose sparing of the rectum and bladder is significantly improved when the non-uniform penalty scheme is employed. Remarkably, the maximum dose to the rectum is reduced from 68 to 60 and the fractional volume is dramatically reduced in the whole dose range. The reduction in the low dose region is more distinct, but the decrease in high dose region is also evident and perhaps more clinically relevant. Similarly significant improvements are achieved in the doses to bladder and femoral heads. For example, the fraction volume receiving a dose of 35 is decreased from 11% to 8% for bladder. The high dose tail in bladder is also evidently suppressed (from 70 to 66). Interestingly, the dose uniformity in the prostate target is also improved: the maximum dose of prostate target is slightly reduced from 110 to 107 and the minimum dose is increased from 85 to 87. In optimization, it is generally true that there is no net gain (that is, an improvement in the dose to a structure is often accompanied by dosimetrically adverse effect(s) at other points in the same or different structures). However, one should note that things may be different when different penalty schemes are used, or more generally, when different objective functions are used. The simultaneous improvements in both

target and sensitive structures here are a direct consequence of the enlarged solution space when non-uniform importance is permissible.

To better understand the technique, we have also optimized the dose under the condition that the non-uniform importance is allowed only for the prostate target (i.e., the importance for all sensitive structures kept uniform). The corresponding isodose distribution is shown in figure 4b and the DVHs are plotted in figure 5 as dotted-dash curves. In this case, it is found that the target dose homogeneity is slightly improved. For example, the fraction receiving over 95 is increased from 91 to 96. The maximum dose is reduced from 110 to 105. By individualizing the importance for the target voxels, we selectively increased the penalties to those voxels that are likely to be underdosed. Consequently, the target dose coverage is improved. It is interesting to note that there is essentially no change in the DVHs of the sensitive structures. The systematic improvement in the isodose distributions when the three different penalty schemes are employed can also be easily appreciated from figure 4.

Five-field IMRT treatment of a paraspinal tumor

The DVHs obtained using the conventional and newly proposed IMRT planning techniques are plotted in Figure 6. The isodose distributions for the two plans are shown in figure 7. Similar to the previous case, when spatially non-uniform importance factors given by Eq. (9) are used, the target dose coverage and sensitive structure sparing are all improved in comparison with the conventional IMRT plan with uniform importance factors. For the target, the improvement is evident especially in the dose range from 90 to 95. The fractional volume receiving dose level of 90 is slightly increased (from 99.3% to 99.7%). A more notable change is found for the fractional volume receiving doses higher than 95 (from 95.1% to 97.5%). The minimum target dose is increased from 84 to 90. The maximum target dose is, however, slightly increased from 105 to 106.5. By using the *a priori* non-uniform penalty scheme, it is found that the doses to the sensitive structures are dramatically improved. As seen from the DVHs, the spinal cord is better spared, especially in the high dose region. For example, the fractional volume of receiving dose above 50 is dropped from 53% to 24%. The fractional volumes of left kidneys receiving a dose above 30 are reduced from 42% to 19% and for the right kidney, the reduction is about 7% (from 17.7% to 10.7%). The improvement for the liver is less impressive but evident. Once again, we would like to

emphasize that the huge improvement in sensitive structure sparing is achieved without significantly deteriorating the dose coverage of the tumor target.

CONCLUSIONS

Inverse planning plays an important role in IMRT and its performance crucially determines the quality of IMRT treatment plans. In this work, we pointed out that voxels within a structure are generally not equivalent in achieving their dosimetric goals and this intrinsic feature should be considered in inverse planning. The concept of dosimetric capability was introduced to quantify the likelihood for a voxel to meet its dosimetric goal and a new inverse planning formalism with customized voxel-dependent penalty was developed. The modulation of local penalty was realized by heuristically relating the local importance factor and the *a priori* dosimetric capability. In this way, we can effectively "boost" those regions where there are potential problems in meeting the dosimetric goals. We would like to mention that using non-uniform importance is not the only way to accomplish a voxel-dependent penalty scheme. Similar effects should also be achievable by modulating the form of the objective function or the prescription value on a voxel-dependent basis. The new formalism provides an effective mechanism to incorporate prior knowledge of the system into the dose optimization process and enables us to better model the intra-structural tradeoff and maneuver the inverse planning process. Comparison of the new formalism with the conventional inverse planning technique for a phantom case and two clinical cases indicated that the algorithm is capable of generating much improved treatment plans with more conformal dose distributions that would otherwise be unattainable. While in this work we have concentrated on the use of a quadratic objective function, the approach proposed here is quite broad and should be applicable for plan optimization based on other types of objective functions to more intelligently model the intra-structural tradeoff. The dosimetric inequivalence of the voxels is a fundamental feature of the system and, regardless the model used, needs to be considered to obtain truly optimal IMRT plans. Finally, we mention that the technique may have many co-lateral applications in dose optimization for many other radiation therapy modalities, such as prostate implantation, gamma knife, micro-MLC based stereotactic radiosurgery, and other variants of IMRT, such as tomotherapy and intensity modulated arc therapy.

Acknowledgments

We would like to thank Dr. Christopher Cameron for carefully reviewing the manuscript. The support from the Department of Defense Breast Cancer Research Program (DAMD17-03-1-0657) is gratefully acknowledged.

REFERENCES

Bedford JL, Cosgrove VP, Tait DM, Dearnaley DP, Webb S. Elimination of importance factors for clinically accurate selection of beam orientations, beam weights and wedge angles in conformal radiation therapy. Proceedings of the Annual San Francisco Cancer Symposium 37: 128-31, 2002.

Bortfeld T, Burkelbach J, Boesecke R, Schlegel W. Methods of image reconstruction from projections applied to conformation radiotherapy. Physics in Medicine & Biology 35 (10): 1423-34, 1990.

Brahme A, Roos JE, Lax I. Solution of an integral equation encountered in rotation therapy. Physics in Medicine & Biology 27 (10): 1221-9, 1982.

Chen Y, Michalski D, Houser C, Galvin JM. A deterministic iterative least-squares algorithm for beam weight optimization in conformal radiotherapy. Physics in Medicine & Biology 47 (10): 1647-58, 2002.

Cho PS, Lee S, Marks RJ, 2nd, Oh S, Sutlief SG, Phillips MH. Optimization of intensity modulated beams with volume constraints using two methods: cost function minimization and projections onto convex sets. Medical Physics 25 (4): 435-43, 1998.

Cotrutz C, Xing L. IMRT dose shaping using regionally variable penalty scheme. Medical Physics 30: 544-551, 2003.

Cotrutz C, Xing L. Using voxel-dependent importance factors for interactive DVH-based dose optimization. Physics in Medicine & Biology 47 (5): 1659-1669, 2002.

Das S, Cullip T, Tracton G, Chang S, Marks L, Anscher M, Rosenman J, Chang SX. Beam orientation selection for intensity-modulated radiation therapy based on target equivalent uniform dose maximization. International Journal of Radiation Oncology, Biology, Physics 55 (1): 215-24, 2003.

Gopal R, Starkschall G. Plan space: Representation of treatment plans in multidimensional space. Medical Physics 28 (6): 1227, 2001.

Holmes T, Mackie TR. A comparison of three inverse treatment planning algorithms. Physics in Medicine & Biology 39 (1): 91-106, 1994.

Hristov DH, Fallone BG. An active set algorithm for treatment planning optimization. Medical Physics 24 (9): 1455-64, 1997.

Langer M, Brown R, Urie M, Leong J, Stracher M, Shapiro J. Large scale optimization of beam weights under dose-volume restrictions. International Journal of Radiation Oncology, Biology, Physics 18 (4): 887-93, 1990.

Langer M, Leong J. Optimization of beam weights under dose-volume restrictions. International Journal of Radiation Oncology, Biology, Physics 13 (8): 1255-60, 1987.

Lian J and Xing L, Incorporating Model Parameter Uncertainty into Inverse Treatment Planning, Medical Physics 31, 2711-2720, 2004.

Michalski D, Xiao Y, Censor Y and Galvin J. The dose-volume constraint satisfaction problem for inverse treatment planning with field segments. Physics in Medicine and Biology 249: 601-616, 2004.

Oelfke U, Bortfeld T. Inverse planning for x-ray rotation therapy: a general solution of the inverse problem. Physics in Medicine & Biology 44 (4): 1089-104, 1999.

Olivera GH, Shepard DM, Reckwerdt PJ, Ruchala K, Zachman J, Fitchard EE, Mackie TR. Maximum likelihood as a common computational framework in tomotherapy. Physics in Medicine & Biology 43 (11): 3277-94, 1998.

Rosen, II, Lam KS, Lane RG, Langer M, Morrill SM. Comparison of simulated annealing algorithms for conformal therapy treatment planning. International Journal of Radiation Oncology, Biology, Physics 33 (5): 1091-9, 1995.

Spirou SV, Chui CS. A gradient inverse planning algorithm with dose-volume constraints. Medical Physics 25 (3): 321-33, 1998.

Starkschall G, Eifel PJ. An interactive beam-weight optimization tool for three-dimensional radiotherapy treatment planning. Medical Physics 19 (1): 155-63, 1992.

Thieke C, Bortfeld T, A. Niemierko and S. Nill. From physical dose constraints to equivalent uniform dose constraints in inverse radiotherapy planning. Med Phys 30: 2332-2339, 2003.

Webb S. Optimization by simulated annealing of three-dimensional conformal treatment planning for radiation fields defined by a multileaf collimator. Physics in Medicine & Biology 36 (9): 1201-26, 1991.

Webb S, Convery DJ, Evans PM. Inverse planning with constraints to generate smoothed intensity-modulated beams. Physics in Medicine & Biology 43 (10): 2785-94, 1998.

Wu C, Olivera GH, Jeraj R, Keller H, Mackie TR. Treatment plan modification using voxel-based weighting factors/dose prescription. Physics in Medicine & Biology 48: 2479-2491, 2003.

Wu Q, Mohan R, Niemierko A, Schmidt-Ullrich R. Optimization of intensity-modulated radiotherapy plans based on the equivalent uniform dose. International Journal of Radiation Oncology, Biology, Physics 52 (1): 224-35, 2002.

Wu X, Zhu Y. An optimization method for importance factors and beam weights based on genetic algorithms for radiotherapy treatment planning. Physics in Medicine & Biology 46 (4): 1085-99, 2001.

Xiao Y, Galvin J, Hossain M, Valicenti R. An optimized forward-planning technique for intensity modulated radiation therapy. Medical Physics 27 (9): 2093-9, 2000.

Xing L, Chen GTY. Iterative algorithms for Inverse treatment planning. Physics in Medicine & Biology 41 (2): 2107-23, 1996.

Xing L, Li JG, Donaldson S, Le QT, Boyer AL. Optimization of importance factors in inverse planning. Physics in Medicine & Biology 44 (10): 2525-36, 1999.

Zagars GK, Starkschall G, Antolak JA, Lee JJ, Huang E, von Eschenbach AC, Kuban DA, Rosen I. Treatment planning using a dose-volume feasibility search algorithm. International Journal of Radiation Oncology, Biology, Physics 53 (5): 1097-105, 2002.

	prostate	bladder	rectum	Femoral heads	skin
importance factor	0.2	0.05	0.1	0.05	0.6
Prescription/tolerance	100	65	60	70	85

Table 1. Summary of the parameters used for planning the IMRT prostate treatment. The tolerances of the sensitive structures are used in the evaluation of the capability maps.

	GTV	Spinal Cord	Liver	Kidney	Tissue
importance factor	0.86	0.03	0.005	0.05	0.055
Prescription/tolerance	100	30	40	30	75

Table 2. Summary of the parameters used for planning the IMRT treatment of the paraspinal tumor. The tolerances of the involved sensitive structures are used in the evaluation of the capability maps.

Figure Caption

Figure 1 Dosimetric capability and importance maps of the target and sensitive structure for a hypothetical case for two beam configurations: (a) the single beam; and (b) five equally spaced beams. The data for each structure is normalized to unity. For visual purpose, the capability and importance maps of the target and sensitive structure are enlarged and shown in the left and right panels for each beam configuration. The lower middle panel of each set of figures shows the complete geometry of the hypothetical structures.

Figure 2 Isodose distributions for plans obtained without (left) and with (right) local importance factor modulation. The isodose curves labeled in the plots are 105% (red), 100% (pink), 80% (yellow), and 40% (blue), respectively.

Figure 3 Target and sensitive structure DVHs corresponding to plans with two different penalty schemes: (a) uniform importance for every structure (dotted-dash curves); and (b) non-uniform importance for both target and sensitive structure (solid curves).

Figure 4 Isodose distributions obtained from three different penalty schemes: (a) uniform importance for every structure; (b) non-uniform importance for the prostate target and uniform importance for other structures; and (c) non-uniform importance for every structure. Red, pink, yellow, and blue curves represent 95%, 80%, 50%, and 35% isodose curves.

Figure 5. Target and sensitive structure DVHs corresponding to plans with two different penalty schemes: (a) uniform importance for every structure (dotted curves); and (b) non-uniform importance for all structures (solid curves).

Figure 6. The comparison of DVHs for paraspinal tumor case between plans obtained from the algorithm proposed, denoted by solid line and plan from conventional optimization, denoted by dotted dash line. The dose sparing of spinal cord, kidney and liver is evidently improved.

Figure 7. Isodose distributions for plans obtained with two different penalty schemes: (a) uniform importance for every structure; and (b) non-uniform importance for every structure. Red, pink, yellow, and blue curves represent 95%, 70%, 55%, and 30% isodose curves.

Figure 1.

(a)

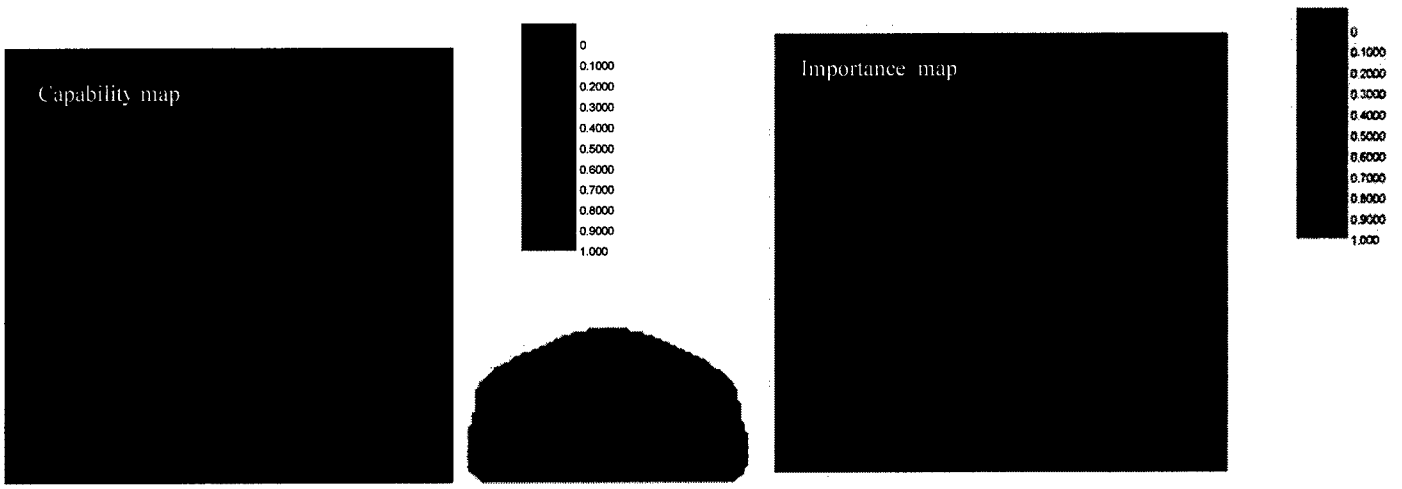
Capability map
0
0.1000
0.2000
0.3000
0.4000
0.5000
0.6000
0.7000
0.8000
0.9000
1.000
Importance map
0
0.1000
0.2000
0.3000
0.4000
0.5000
0.6000
0.7000
0.8000
0.9000
1.000

(b)

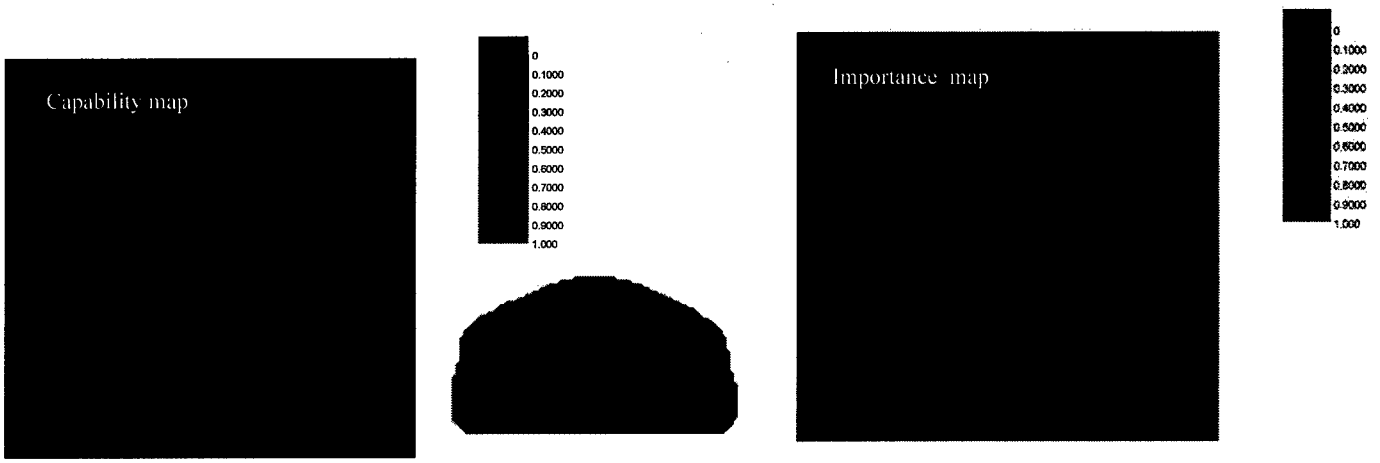
Capability map
0
0.1000
0.2000
0.3000
0.4000
0.5000
0.6000
0.7000
0.8000
0.9000
1.000
Importance map
0
0.1000
0.2000
0.3000
0.4000
0.5000
0.6000
0.7000
0.8000
0.9000
1.000

Figure 2.

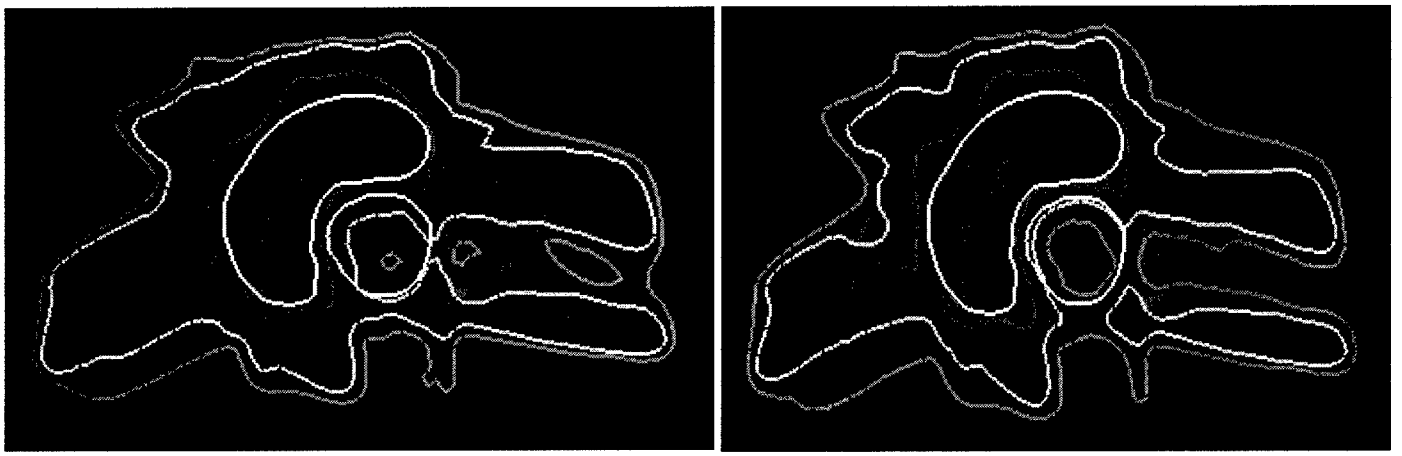

Figure 3.

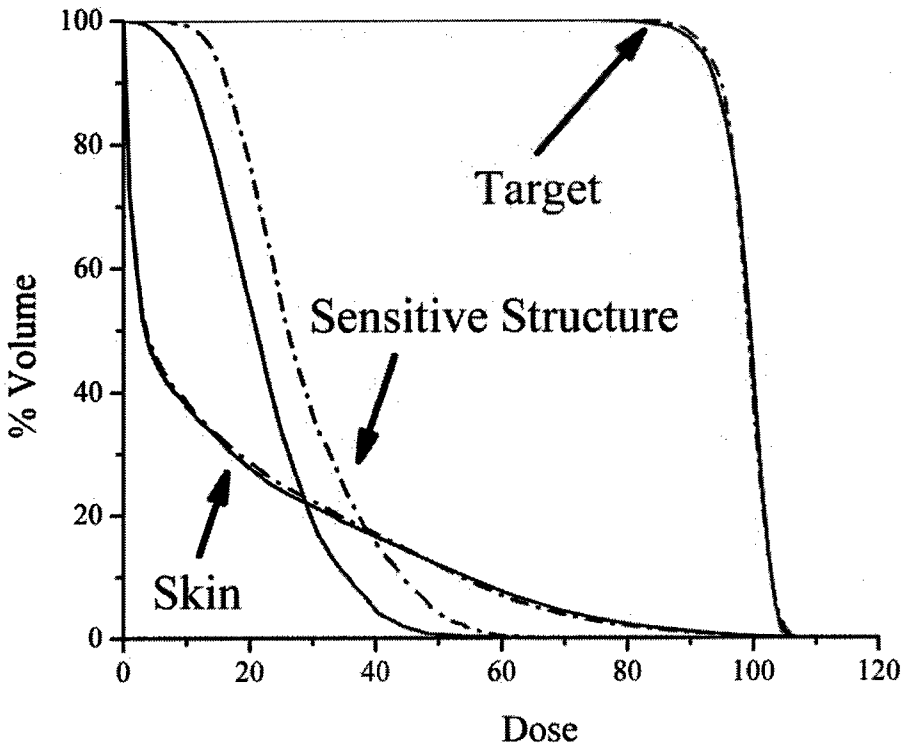
100
80
60
40
20
0
% Volume
0
20
40
60
80
100
120
Dose
Target
Sensitive Structure
Skin

Figure 4.

(a)

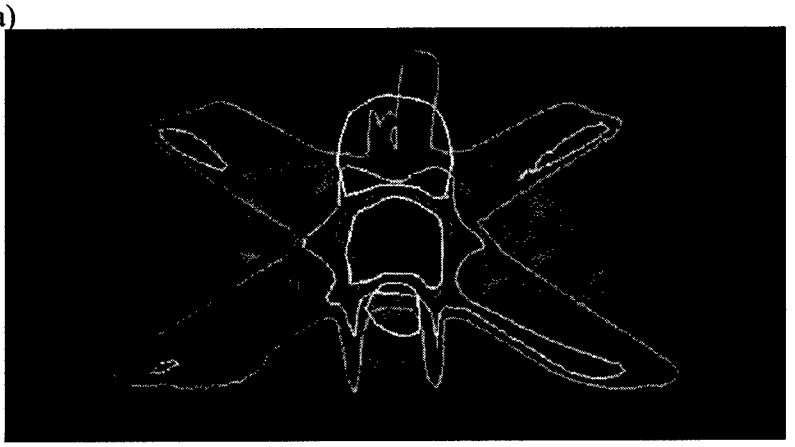

(b)

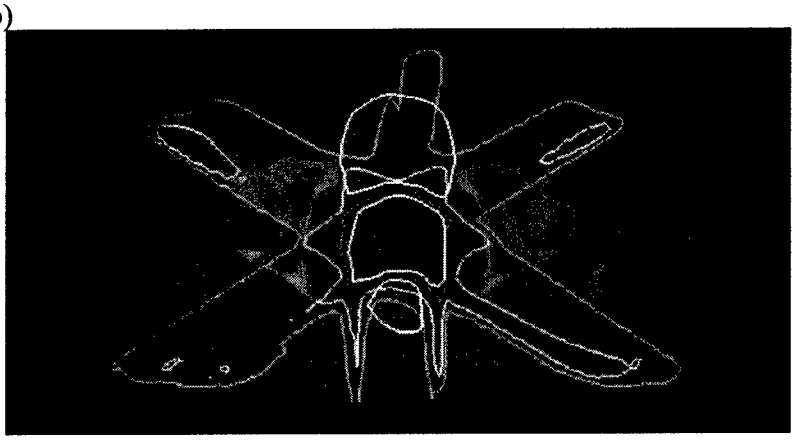

(c)

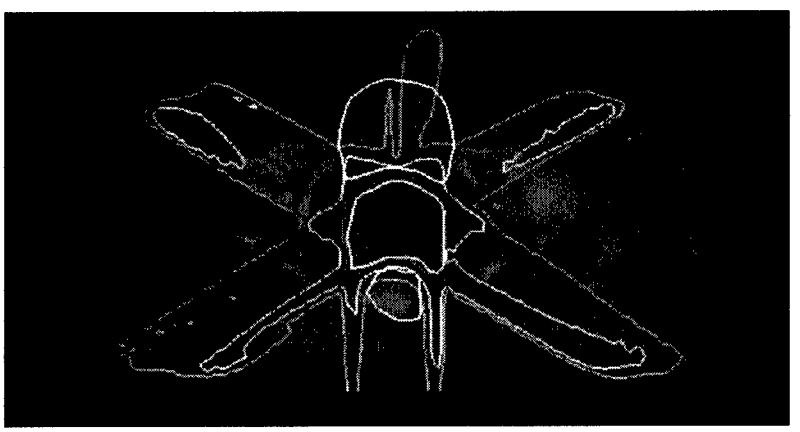

Figure 5

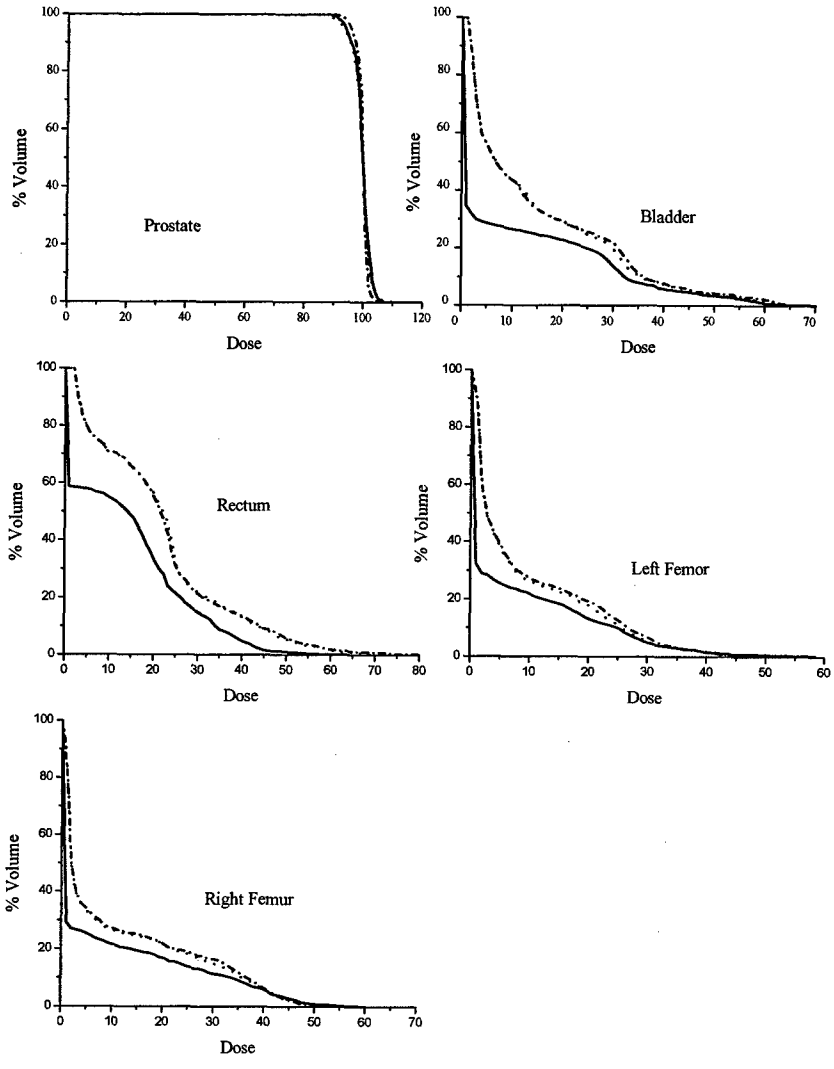
% Volume
Prostate
Dose
% Volume
Bladder
Dose
% Volume
Rectum
Dose
% Volume
Left Femor
Dose
% Volume
Right Femur
Dose

Figure 6

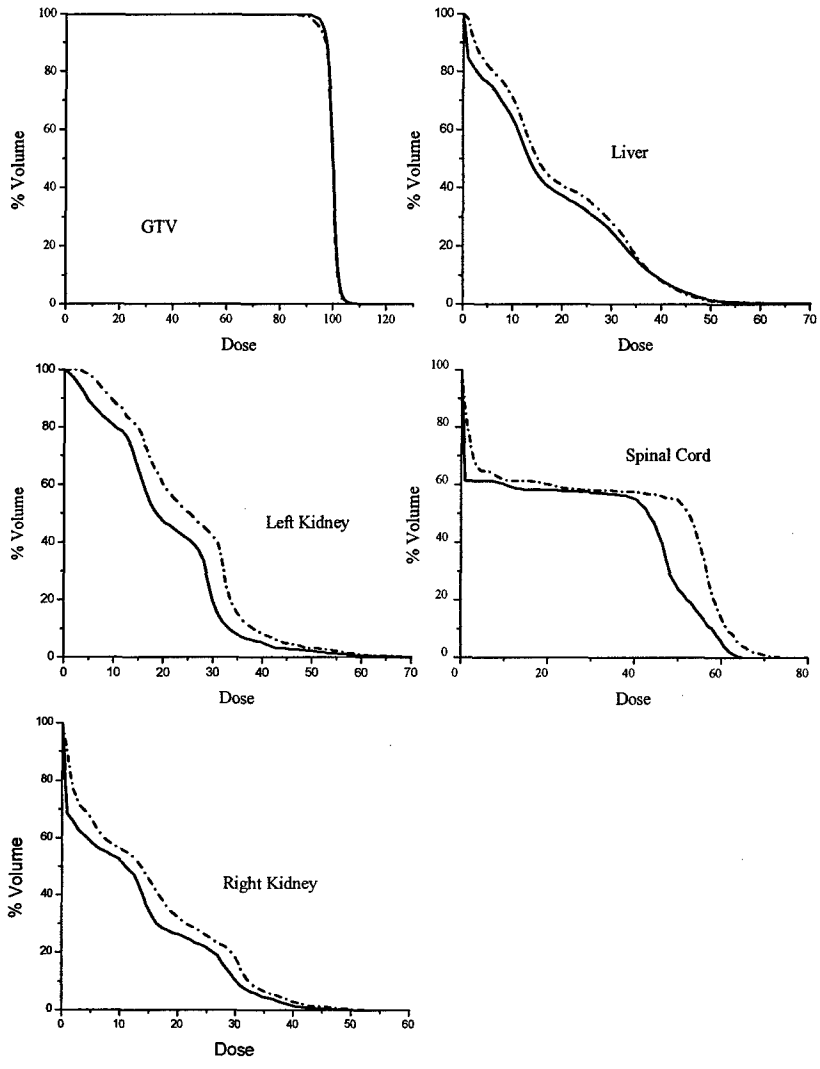

Figure 7

(a)

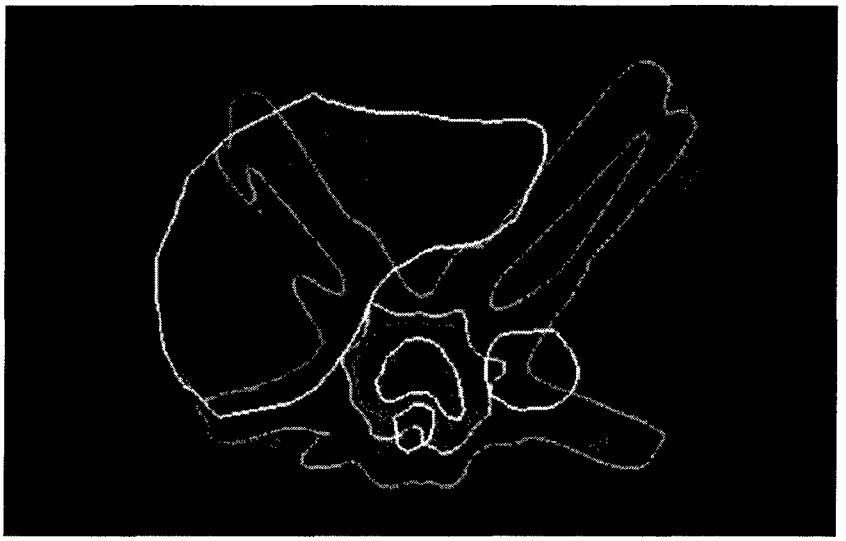

(b)